AGU PUBLICATIONS

JGR

Journal of Geophysical Research: Atmospheres

RESEARCH ARTICLE
10.1002/2013JD020410

Key Points:
- Synoptic warming aloft is the primary force for buildup of persistent cold air pool
- WRF adequately simulates the buildup/breakup of persistent cold air pool
- Midwinter lake breeze can recharge cold air pool with cold and moist air

Correspondence to:
S. Zhong,
zhongs@msu.edu

Citation:
Lu, W., and S. Zhong (2014), A numerical study of a persistent cold air pool episode in the Salt Lake Valley, Utah, *J. Geophys. Res. Atmos.*, *119*, 1733–1752, doi:10.1002/2013JD020410.

Received 23 JUN 2013
Accepted 24 JAN 2014
Accepted article online 31 JAN 2014
Published online 25 FEB 2014

A numerical study of a persistent cold air pool episode in the Salt Lake Valley, Utah

Wei Lu[1] and Shiyuan Zhong[1]

[1]Department of Geography, Michigan State University, East Lansing, Michigan, USA

Abstract The Weather Research and Forecasting (WRF) model is used to simulate a persistent cold air pool (CAP) episode observed in December 2010 during the Persistent Cold Air Pool Study (PCAPS) field campaign in Salt Lake Valley, Utah. The availability of intensive observations from PCAPS, especially the added vertical profiles, allows for an in-depth analysis of CAP structure and evolution and model evaluation beyond what was done in similar work before. Comparisons of the WRF simulation with surface observations and upper air soundings indicate that WRF is capable of simulating the observed spatial and temporal variation of the valley atmosphere during the CAP episode. The model also successfully captures the formation and removal of the persistent temperature inversion. Process analysis helps quantify the contribution of various physical processes to the buildup and breakup of the inversion. The inversion developed due primarily to a rapid warming above the valley by synoptic subsidence and warm advection and to strong radiative cooling within the valley under clear sky conditions. The inversion was lifted when strong southerly winds entered the valley from the gap mixing out the cold air in the valley. Synoptic-scale cold advection above the valley contributed to the inversion removal by weakening the inversion from aloft. Sensitivity experiments suggested that the WRF simulation of the CAP episode is more sensitive to large-scale initialization fields with North American Mesoscale Model outperforming North American Regional Reanalysis and National Centers for Environmental Prediction (NCEP) Eta analysis than to the choice of boundary layer parameterizations and land surface models.

1. Introduction

A cold air pool (CAP) is a topographically confined, stagnant layer of air that is colder than the air above [*Whiteman et al*., 2001]. A CAP can fall into one of the two categories: diurnal CAPs that develop at night and break up the next morning, and persistent CAPs that last longer than a diurnal cycle. While diurnal CAPs are observed year round, the persistent CAPs occur primarily in the winter season. Because persistent CAPs tend to trap air in topographically confined regions for periods spanning from days to weeks, they are often associated with degraded air quality, visibility, and deteriorated transport conditions that are difficult to forecast in populated valleys and basins [*Hill*, 1993; *Pataki et al*., 2005; *Silcox et al*., 2012; *Smith et al*., 1997; *Struthwolf*, 2005].

CAPs have been observed in basins and valleys and other types of terrain depressions in countries with large alpine regions, including Japan [*Kondo et al*., 1989; *Kudoh et al*., 1982; *Magono et al*., 1982; *Nakamura and Magono*, 1982], Slovenia and Croatia [*Petkovsek*, 1978, 1980, 1992; *Vrhovec*, 1991], Austria [*Eisenbach et al*., 2003; *Steinacker et al*., 2007; *Whiteman et al*., 2004a, 2004b, 2004c], New Zealand [*Kossmann et al*., 2002; *Sturman et al*., 2003a, 2003b], Canada [*Sakiyama*, 1990], and the United States [*Allwine et al*., 1992; *Banta*, 1984; *Clements et al*., 2003; *Reeves and Stensrud*, 2009; *Whiteman et al*., 1999, 2008; *Wolyn and Mckee*, 1989; *Yao and Zhong*, 2009]. Because of the difficulty in making long-term field observations in harsh wintertime condition in mountainous terrain, the majority of the observational studies have focused on the characteristics of the diurnal CAPs and the processes leading to their formation and removal. A limited number of studies have investigated persistent CAP properties and processes involved in their formation and destruction by using either twice daily standard sounding data or data collected during multiday field experiments.

In addition to the observational challenges, CAPs also pose significant challenges to numerical models because of their association with complex topography and statically stable atmospheric conditions. Most numerical studies on CAPs [*Anquetin et al*., 1998; *Bader and McKee*, 1983, 1985; *Rakovec et al*., 2002; *Vrhovec*, 1991; *Vrhovec and Hrabar*, 1996; *Zängl*, 2003, 2005a, 2005b, 2005c] have employed idealized topography and/or physical configurations. Only a few studies [*Billings et al*., 2006; *Smith et al*., 2010; *Wei et al*., 2013; *Zhong et al*., 2001] have attempted to simulate real-world CAP episodes using realistic terrain and atmospheric conditions.

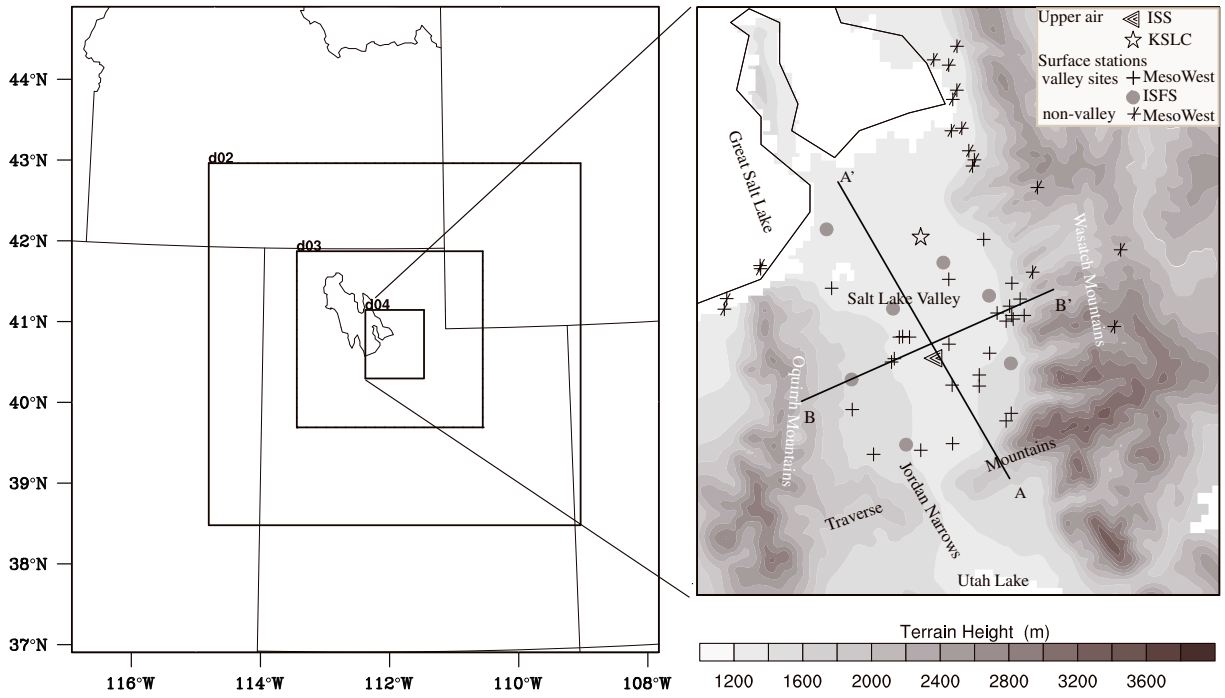

Figure 1. The WRF model domain setup, topography of the innermost domain, and the observational sites used in the study. The lines AA' and BB' are the horizontal positions of along-valley and cross-valley vertical cross sections discussed in the text.

Recently, an intensive field campaign called the Persistent Cold Air Pool Study (PCAPS) was conducted between 1 December 2010 and 7 February 2011 in Utah's Salt Lake Valley [*Lareau et al.*, 2013]. The nearly 2 month long midwinter field campaign captured 10 persistent CAP episodes with an extensive suite of spatiotemporal observations, thus providing an unprecedented opportunity to better understand the processes involved in persistent CAP formation and breakup. In the current study, the Weather Research and Forecasting Model (WRF) [*Skamarock et al.*, 2005] is used to simulate one of the persistent CAP episodes observed during PCAPS. The objectives of the study are twofold: to evaluate the skill of the WRF model in simulating the observed structure and evolution of a persistent CAP and determine an optimal set of model configuration and physical parameterizations and to better understand the physical mechanisms behind CAP development and removal. A recent study [*Wei et al.*, 2013] also used the WRF model to simulate a persistent CAP episode in the Salt Lake City, but the data used to validate the simulation was limited to routine observations. The twice daily rawinsonde soundings from the Salt Lake City, which was the only upper air data used in the study, lack the temporal resolution to depict the details in the boundary layer evolution. In addition, the WRF simulation used relatively coarse horizontal resolution (1.3 km) that does not resolve well the canyons and tributaries in the mountain ranges bordering the valley. The current study attempts to overcome these shortcomings. The rest of the paper is constructed as follows: the persistent CAP episode observed during PCAPS is presented in section 2, the model configuration is described in section 3, results and discussion are presented in section 4, and the paper is concluded in section 5.

2. Description of the Site, Data, and Case

The area of interest in this study is Utah's Salt Lake Valley. The Salt Lake Valley lies in north central Utah on the eastern edge of the Great Basin with an average elevation of 1320 m above mean sea level (msl). The valley is surrounded by steep mountains in all directions except the northwest: Oquirrh Mountains (rise approximately to about 3000 msl) to the west, Wasatch Range (rises to about 3500 msl) to the east, and the lower Traverse Range to the south, with a gap in the Traverse Range known as the Jordan Narrows connecting the Salt Lake Valley with the Utah valley to the south. The floor of the Salt Lake Valley slopes slightly downward from south (~1392 msl) to north (~1282 msl) with the Great Salt Lake at the lowest elevation in the northwest portion of the valley (Figure 1).

During the PCAPS field campaign, hourly surface meteorological data were obtained from more than 100 observing sites scattered across the valley and the surrounding mountains representing varying topography and land use. The sites were composed of preexisting stations in the MesoWest network [*Horel et al*., 2002] and seven additional PCAPS sites that were equipped with National Center for Atmospheric Research's (NCAR) Integrated Surface Flux Station. The latter provided measurements of radiation and turbulence as well as soil heat and moisture fluxes in addition to standard surface weather variables. Above the surface, the observational data included half-hourly wind and virtual temperature profiles from a 915 MHz radar wind profiler and radio acoustic sounding system (RASS) as part of NCAR's Integrated Sounding System (ISS) located on the valley floor near the center of the valley. Also, rawinsondes were launched at 3-hourly intervals from ISS during periods of rapid transition and twice daily at 00Z (17 MST) and 12Z (0500 MST) from the Salt Lake City International Airport (KSLC). The type of sites and their locations are shown in Figure 1. More detailed description about the PCAPS campaign, the instruments used, and the observational data can be found in *Lareau et al*. [2013].

The period of this study spans from 12 to 15 December 2012, which encompassed the third Intensive Observation Period (IOP3) of the PCAPS field campaign. During this period, there was no evidence of widespread snow cover on the ground, which was different from the CAP episode in *Wei et al*.'s [2013] study. Because of the high salinity, there is never permanent ice pack over most of Great Salt Lake except for occasional ice cover in the Farmington Bay and areas surrounding it. The lake temperature during the study period was a few degrees above freezing, and no ice was present over any part of the Great Salt Lake.

The synoptic conditions during the study period are depicted in Figure 2 with 700 hPa geopotential height fields and wind vectors from the North American Mesoscale Model (NAM) analyses; the 700 hPa level is near the ridge top level of the Salt Lake Valley. On 11 December, the day before IOP3 officially started, a high resided to the west of the Pacific coast and a cutoff low was present over the upper Great Plains, contributing to moderate northwesterly winds in the Intermountain West (Figure 2a). The northwesterly flow transported colder air from higher latitudes into the Intermountain West which formed the basis for the development of the persistent CAP. On the following day, the high and the associated ridge moved slowly eastward while expanding in size to cover most of the western U.S. (Figures 2b–2d). Associated with the inland movement of the ridge was a rapid warming over the Intermountain West as warm air was advected from the south-southwest into the region and synoptic subsidence strengthened (Figures 2c and 2d). As the ridge moved farther inland, its strength weakened while a shortwave trough began to develop off the coast of the Pacific Northwest (Figures 2e and 2f). On 14 December, the ridge was further flattened by the trough, with generally zonal flow present over the region. Finally, the trough deepened on 15 December, bringing cold air advection aloft to the region. The synoptic setting in this case is similar to the synoptic conditions in the conceptual model for valley CAPs developed by *Reeves and Stensrud* [2009], based on climatological analyses of valley CAPs during a 3 year period.

The PCAPS surface and upper air observations depict the development of this CAP event (not shown), but despite its advantages over routine observational networks (e.g., temporal frequency), the PCAPS observations are still insufficient to fully understand the three-dimensional structure of the CAP and the relative role of local and synoptic-scale forcing in the formation and breakup of this episode. Thus, high-resolution numerical simulations are performed to help facilitate understanding. Furthermore, the simulations allow for an assessment of the skill of the model in forecasting the formation, duration, and breakup of persistent CAPs.

3. Description of the Model and Numerical Experiments

3.1. Model and Grid Configuration

The WRF model version 3.0 was employed for the numerical simulations. As described in section 2, the Salt Lake Valley is surrounded by mountains with steep slopes and narrow canyons and mountain gaps. To resolve the highly variable topography, the WRF model is configured with four one-way nested grids with grid spacing decreasing from 13.5 km in the outermost grid, to 1.5 and 4.5 km in the two intermediate grids, and finally to 500 m in the innermost grid. The location of each grid is shown in Figure 1 along with the model topography in the innermost grid. All domains utilized 45 vertical levels stretched from the surface to 50 hPa. Damping was employed at the model top to prevent wave reflection from the upper boundary.

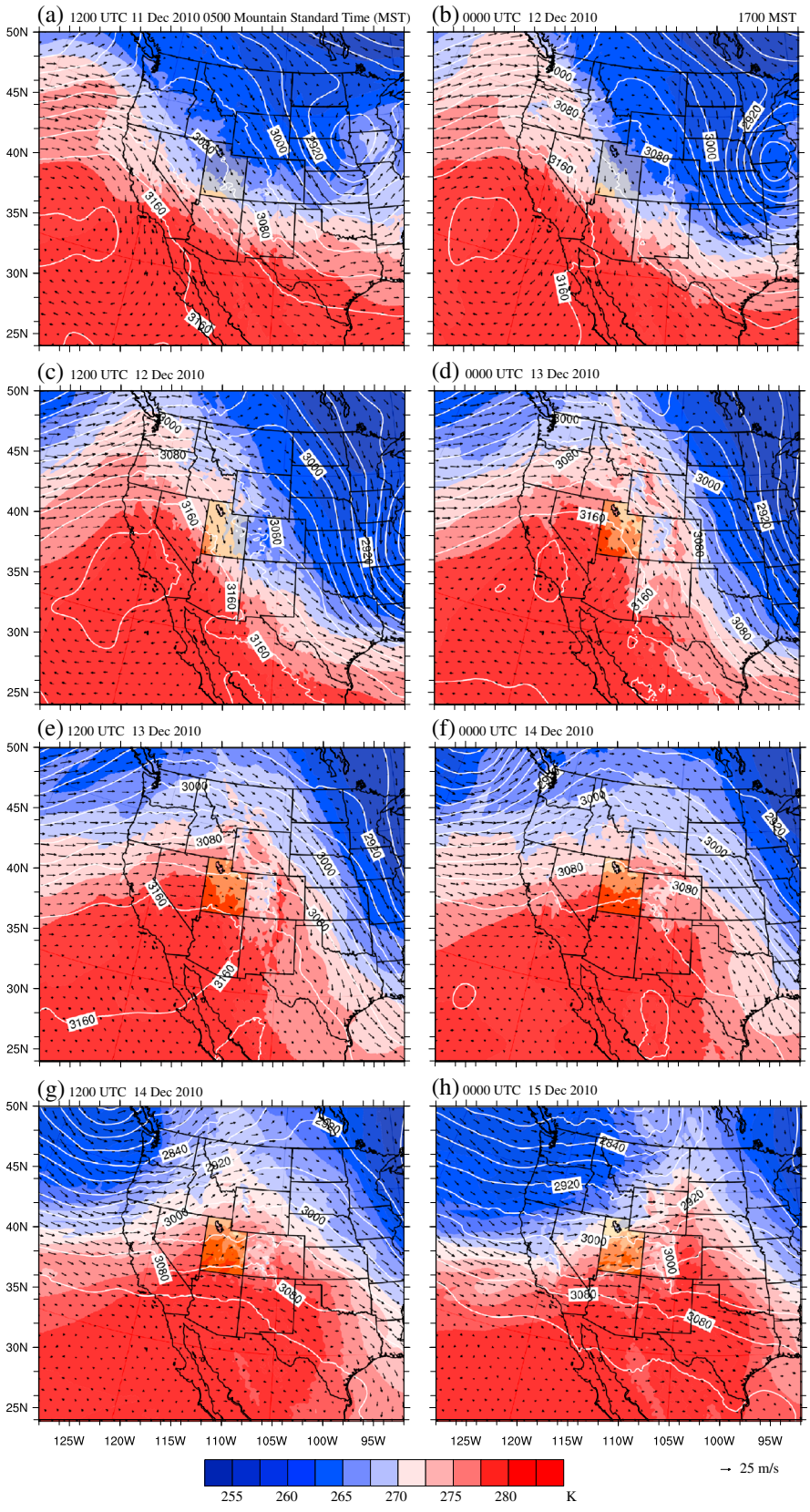

Figure 2. The 0000 UTC and 1200 UTC NAM analyses of the 700 hPa geopotential height, potential temperature, and wind vector for the simulation period from 11 December through 15 December. The state of Utah is distinguished by shade of yellow.

Table 1. Summary of Physics Options and Large-Scale Data Sets Used in the Sensitivity Study

Initialization	Boundary Layer Schemes	Land Surface Model
North American Mesoscale (NAM) model (12 km resolution at 6 h intervals)	Mellor-Yamada-Janjic (MYJ) [*Janjic*, 1990, 1994, 2001; *Mellor and Yamada*, 1982]; local closure scheme	Rapid Update Cycle (RUC) [*Smirnova et al.*, 2000]; layer approach to energy and moisture budget; six levels in the soil at 0, 5, 20, 40, 160, and 300 cm; multilayer snow model
NARR (32 km resolution at 3 h intervals)	Yonsei University (YSU) [*Hong et al.*, 2006]; nonlocal scheme	Noah [*Chen and Dudhia*, 2001], four soil layers of 10, 30, 60, and 100 cm thickness; one snow layer with fractional snow coverage
ETA (40 km resolution at 6 h intervals)		
NAM-, NARR-, ETA-	MYJ, YSU	-RUC, -Noah

3.2. Numerical Experiment

As a community model for multiscale applications, the WRF model offers a range of user-determined options that deals with many aspects of the model from large-scale data sets for driving regional simulations and land-surface models, to physical parameterization schemes and numerical schemes. While the primary purpose of the current study is to help depict the three-dimensional structure and evolution of the persistent CAPs and provide better understanding of the forcing, a secondary objective is to take advantage of enhanced observations from PCAPS to assess the skill of WRF in forecasting CAPs and identify an optimal set of model parameters to achieve the best forecast. For this purpose, a series of seven simulations were carried out with varying combinations of planetary boundary layer (PBL) parameterization schemes (Mellor-Yamada-Janjic (MYJ) and the Yonsei University (YSU)), land surface models (LSM) (Noah LSM (Noah) and Rapid Update Cycle (RUC)) and large-scale data sets (the North American Mesoscale Model (NAM), North American Regional Reanalysis (NARR), and the NCEP ETA model) for model initialization/lateral boundary conditions. Table 1 briefs the major differences among the schemes and the data sets used in the simulations. The physical packages differ in assumptions in each scheme. Compared to the MYJ PBL scheme, the YSU scheme permits mixing beyond adjacent levels by introducing a nonlocal term. The RUC LSM has higher vertical resolution and thinner top layers in soil models and a more complex snow scheme than what are in the Noah LSM. The three large-scale data sets used for initialization and boundary condition differ in a number of aspects including the model, the observational data assimilated, and the temporal and spatial resolution. For detailed descriptions of these schemes and data sets, refer to the citations in Table 1.

All simulations were initialized at 1200 UTC 11 December and run through 0000 UTC 15 December.

4. Results and Discussions

We will first focus our discussions on one of the seven simulations listed in Table 1: NAM-MYJ-RUC. The sensitivity of the results to model parameterizations and initializations will be discussed at the end of this section. All discussions refer to results from the finest resolution (500 m) grid over the 3 day period from 0000 UTC 12 December through 0000 UTC 15 December excluding the first 12 h after the initialization to allow sufficient time for model spin-up. To aid the discussion, mountain standard time (MST) is 7 h behind UTC and sunrise is around 0740 MST (1440 UTC) while sunset is around 1700 MST (0000 UTC).

4.1. Model Validation

The model results are first compared to the PCAPS observations during this CAP episode in order to assess how well the WRF model captures the observed spatial and temporal variation of the near-surface meteorological fields as well as the boundary layer structure and evolution.

The simulated and observed near-surface temperature distributions across the Salt Lake Valley and the surrounding mountain ranges and their time evolution are shown in Figure 3. Several features emerge from the observations. First, a comparison of nighttime (Figures 3a, 3b, 3e, 3f, 3i, and 3j) with daytime (Figures 3c, 3d, 3g, 3h, 3k, and 3l) patterns reveals diurnal variations in the surface air temperature with larger amplitude inside the valley compared to the surrounding high terrain. Second, a comparison of day-to-day variations suggests a gradual warming trend through the CAP episode, with colder temperatures early in the period and much warmer temperatures toward the end of the episode, which is consistent with the synoptic analyses discussed earlier (Figure 2). Note that the model reproduces the observed diurnal cycle and the general warming trend through the period. However, the increase in morning temperature appears to be weaker in

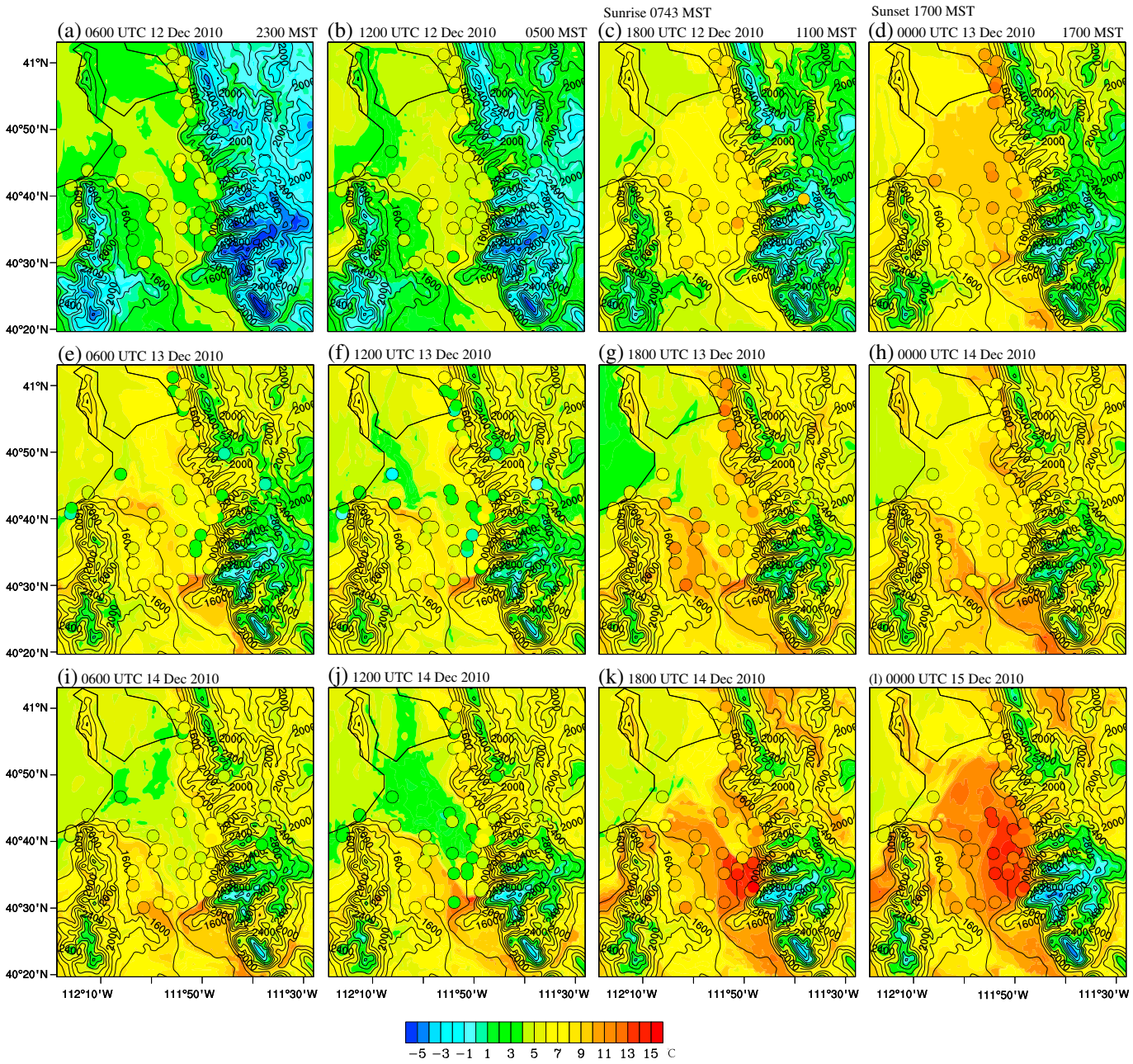

Figure 3. Simulated (shading) and observed (circle) 2 m temperature for (a, b, e, f, i, and j) nighttime and (c, d, g, h, k, and l) daytime in the innermost model domain over the Salt Lake Valley. The contours are terrain height (200 m interval).

the model results, leading to an underestimation around noon (Figures 3c, 3g, and 3k). However, the simulation appears to catch up with the observations in the afternoon hours, as reflected by the somewhat better agreement in the late afternoon (Figures 3d, 3h, and 3l). The nighttime cooling is underestimated by the model, a feature that has also been reported from simulations of persistent valley CAPs in the Bonneville Basin using the NAM model [*Reeves et al.*, 2011]. The simulation captures the observed spatial pattern which appears to be a function of elevation and the distance from the Great Salt Lake.

The surface winds in the valley also varied considerably through the period (Figure 4). Early on (Figures 4a–4e, 0600 UTC December 1200–0600 UTC December 13), southerly winds prevailed in the valley except for the areas near the foothills of the Wasatch Front where winds were weak and variable. The weak winds extended to the rest of the valley during the middle period (Figures 4f–4j, 1200 UTC December 13–1200 UTC December

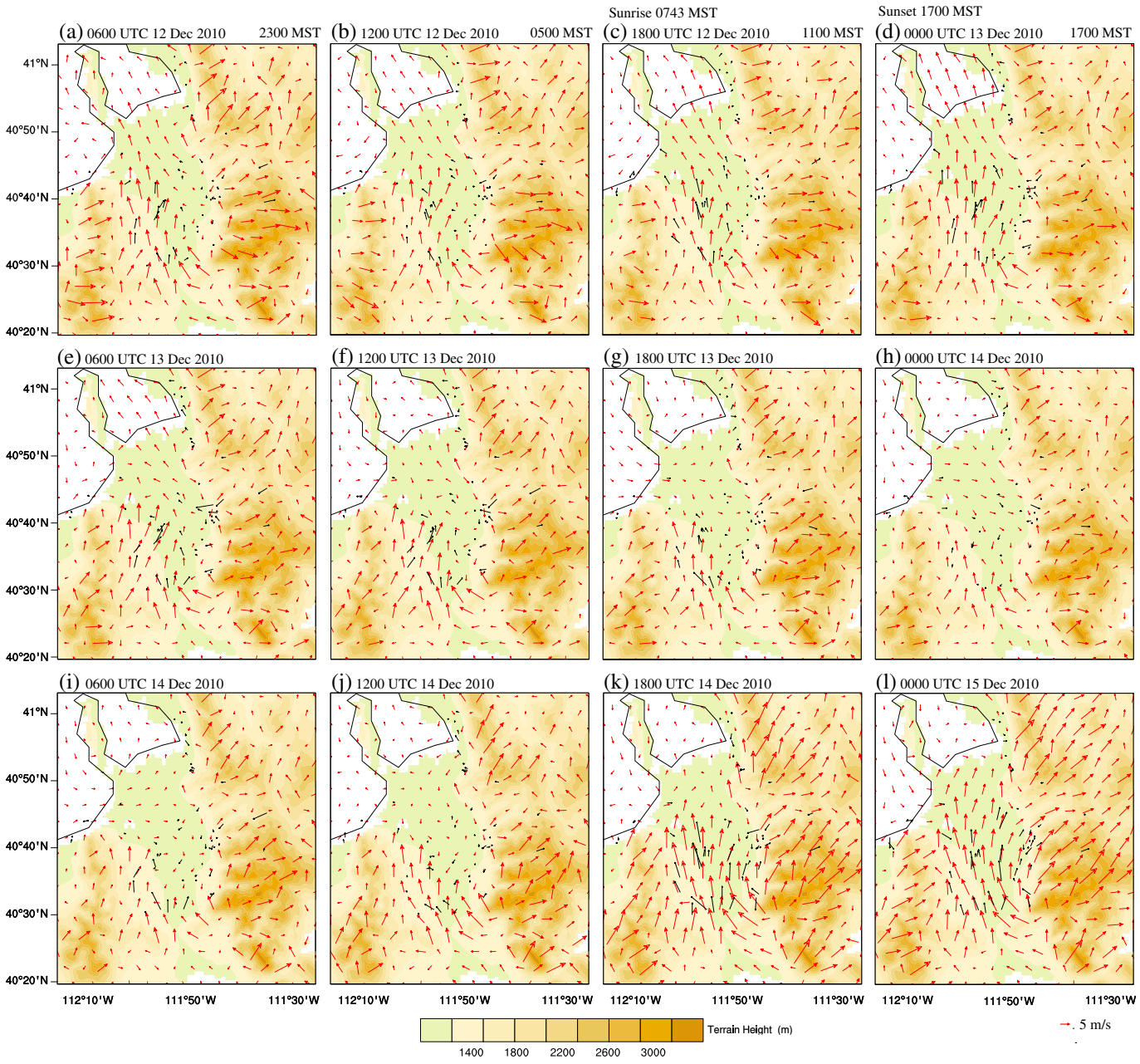

Figure 4. The same as Figure 3 but for simulated (red) and observed (black) surface wind vectors.

14) with the southerly winds retreating to the Oquirrh Mountains and Jordan Narrow. The near-calm condition in the valley allowed for the development of a lake breeze from the Great Salt Lake in the afternoon of 13 December (Figure 4g and 4h). A lake breeze is uncommon on a midwinter day, which will be discussed in more detail in the next section. Near the end of the period (Figure 4k and 4l, 1800 UTC 14 December to 0000 UTC 15 December), southerly winds once again became strong and propagated from the south-southwest across the valley to reach the Great Salt Lake in the northern end of the valley.

The southerly winds simulated by WRF in Figure 4 are stronger than the observed winds at some sites in the early stage of the CAP event, and they also occupy a larger area near the Oquirrh Mountains. However, the quiescent period is captured by the model as well as the lake breeze during the afternoon of 13 December. At the end of the simulation, the simulated southerly wind intrusion is stronger and occurred earlier than was observed, which is also reflected in the comparison of the simulated and observed temperature fields (Figure 3).

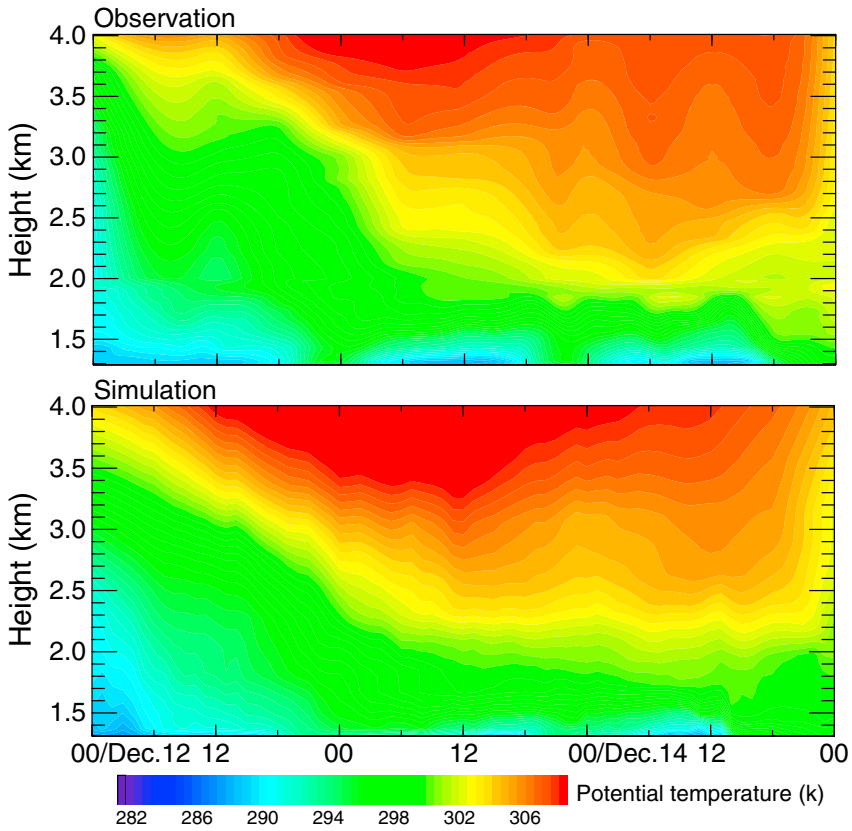

Figure 5. Time-height cross section of the (top) observed and (bottom) simulated potential temperatures at the ISS site from 0000 UTC 12 December through 0000 UTC December 15.

A comparison of simulated and observed boundary layer structure and evolution reveals the degree to which the model is capable of capturing the formation and removal of the temperature inversion in the valley. Figures 5 and 6 show simulated and observed time-height cross sections of potential temperature and wind vectors at the ISS site near the center of the valley (Figure 1). The observed temperature and winds were obtained from a 915 MHz radar wind profiler/RASS and the model output was extracted from the grid point nearest to the ISS site. The radar wind profiler provided wind from approximately 200 m to 3000 m above ground level (agl) while the RASS provided virtual temperature profiles from approximately 100 to 1000 m agl. In order to compare modeled and observed temperature structure over the depth of the valley boundary layer, the rawinsonde temperature data have been used to extend the vertical coverage of RASS from 1 km to 4 km.

During the first day of the simulation period (0000 UTC 12 December to 0000 UTC 13 December), a rapid warming occurs above the valley with potential temperature increasing by 8–10 K in 24 h. Accompanying this warming is a rapid descent of a subsidence inversion from about 4 km msl to the top of the valley (~3000–3500 m msl). In the period that follows (0600 UTC 13 December to 1800 UTC 14 December), the subsidence inversion slowly descends into the upper part of the valley and remains there through the rest of the period, while the rapid warming in the upper part of the valley and above the valley is replaced by a wavy potential temperature pattern. Finally, beginning around 1800 UTC 14 December, the air in the upper part of the valley and above experiences a rapid cooling that ends with the lifting of the subsidence inversion around 0000 UTC 15 December. Inside the valley, a deep layer of cold air is present at the beginning of the period; however, later in the period the cold air is limited to the lowest 200–300 m above the valley floor. A weak diurnal cycle is evident within the lowest 200 m agl with a surface-based inversion at night which is replaced by a near-neutral atmosphere during the day. Above the layer of the diurnal cycle, the valley atmosphere remains near neutral to slightly stable. Beginning at 1800 UTC 14 December, a warming phase occurs in the lower valley and midvalley atmosphere.

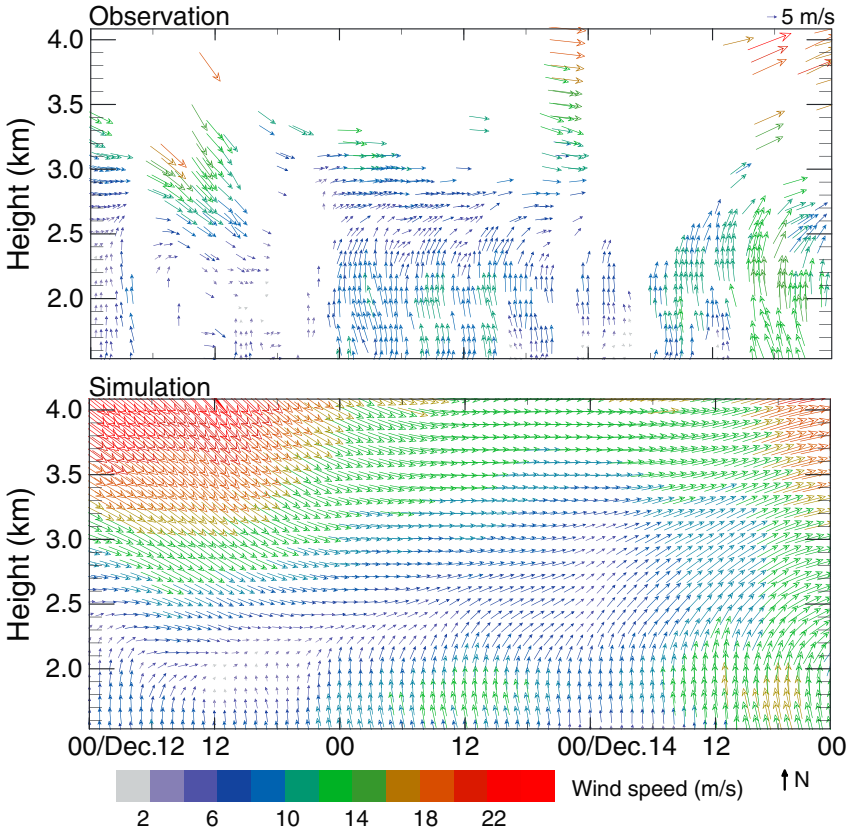

Figure 6. The same as Figure 5 but for (top) observed and (bottom) simulated hourly horizontal wind vectors.

Although there is a relatively well-defined end to the persistent inversion and CAP episode around 0000 UTC 15 December as the inversion is lifted up and the valley is mixed out, identification of the beginning of this episode, however, is less certain. Whereas definitions of a CAP have been put forward by different investigators [e.g., *Petkovsek*, 1992; *Whiteman et al*., 2001; *Reeves and Stensrud*, 2009], there is no official definition of what exactly constitutes a CAP in the literature. Here we define the beginning of this particular CAP episode as 1200 UTC 12 December, when the inversion reaches the top of the Wasatch Mountain (~3500 m msl). This time coincides with the start time of IOP3 [*Lareau et al*., 2013] although the latter has more to do with the commencement of enhanced operations (e.g., more frequent rawinsondes launches) and is not tied to any physical definition of CAPs.

A careful comparison of the simulated and observed vertical potential temperature structure and evolution (Figure 5) shows that the model successfully captures the strengthening and descending of the subsidence inversion above the valley during the initial phase and the lifting of the inversion at the end. The model also simulates the observed diurnal cycle in the lowest 200 m above valley floor and the temperature variation and stratification in the bulk of the valley atmosphere. The nocturnal cooling is underestimated in the simulation, and the warming of the lower valley near the end of the period is also somewhat weaker compared to the observations. Overall, the simulated CAP evolution is in good agreement with the observations.

The observed wind vectors (Figure 6 (top)) reveal complex structures in the valley boundary layer. The prevailing winds in the valley were generally southerly in the lowest 1000 m above valley floor. The strength of the southerly flow exhibited a diurnal oscillation, stronger at night and weaker during the day, due possibly to the superposition of the thermally driven valley flow that is southerly (down valley) at night and northerly (up valley) during the day. Despite the diurnal variation, the southerly winds in the lower part of the valley were weak with speeds less than 5 m s^{-1} until the late morning of 14 December when strong southerly winds of 8 m s^{-1} or stronger occupied the depth of the valley. In the upper part of the valley and the layer above the valley, the winds were northwesterly on the first day of the simulation (0000 UTC 12 December to 0000 UTC 13 December), becoming westerly on the following day, and finally switching to west southwesterly on the last day.

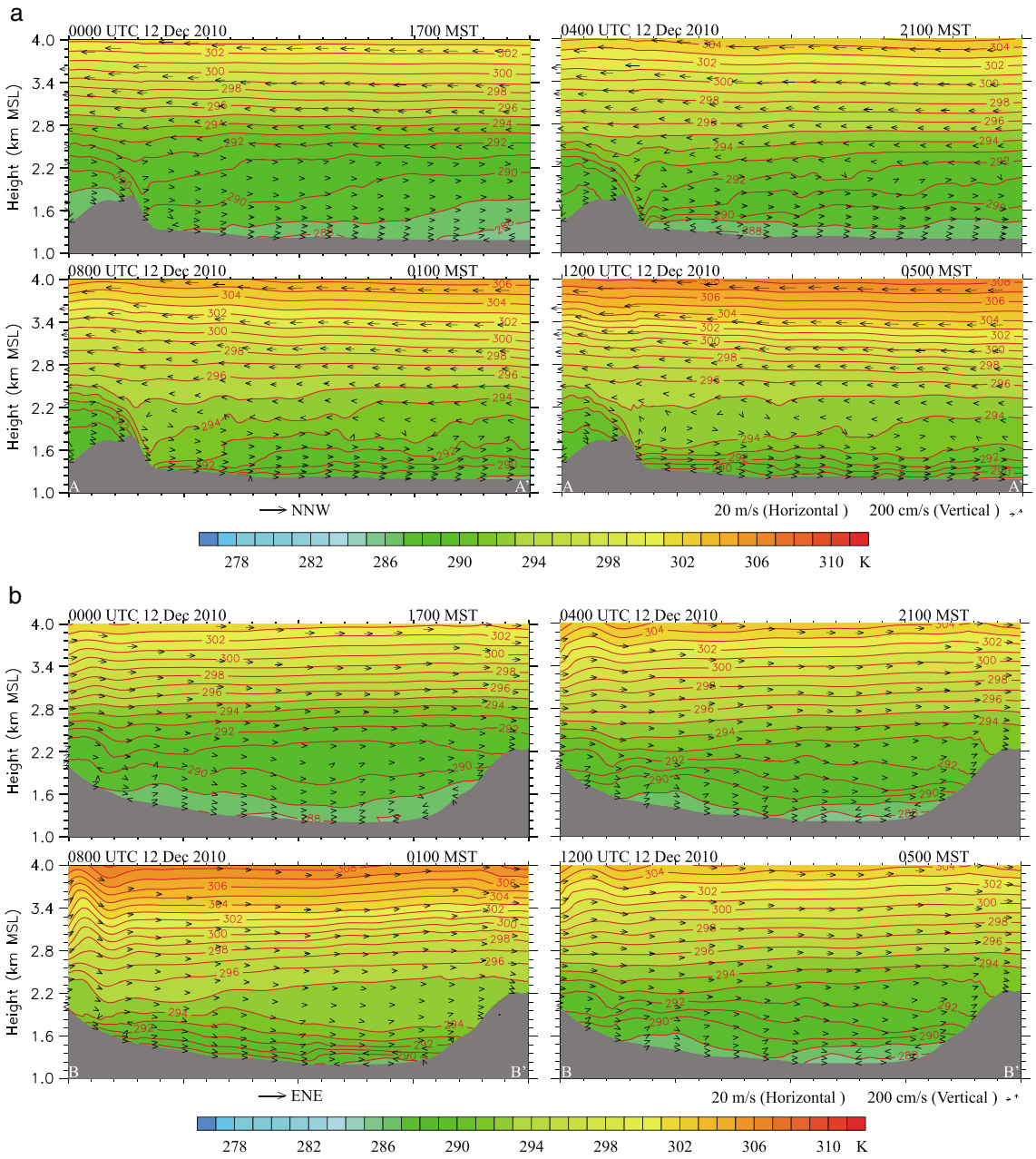

Figure 7. Cross section along (a) AA′ and (b) BB′ of modeled potential temperature (contours of every 1 K) and wind vectors projected on the cross-sectional plane during the buildup state of the cold air pool.

The model captures the transition of wind speed and direction from within the valley to above the valley. The simulated direction changes with height and time are in very good agreement with the observed changes, but the simulated wind speeds are slightly stronger within the valley than what was observed.

Overall, the model appears to capture the observed CAP evolution and boundary layer structure reasonably well. With confidence in the model results, we now proceed to a more detailed examination of the CAP structure and the physical processes involved in the buildup and breakup of the CAP using the results from the simulation.

4.2. CAP Structure and Evolution

To aid the discussion, the entire CAP episode is divided subjectively into three stages: the buildup stage (0000 UTC 12 December to 0000 UTC 13 December) when the subsidence inversion descends rapidly to the top

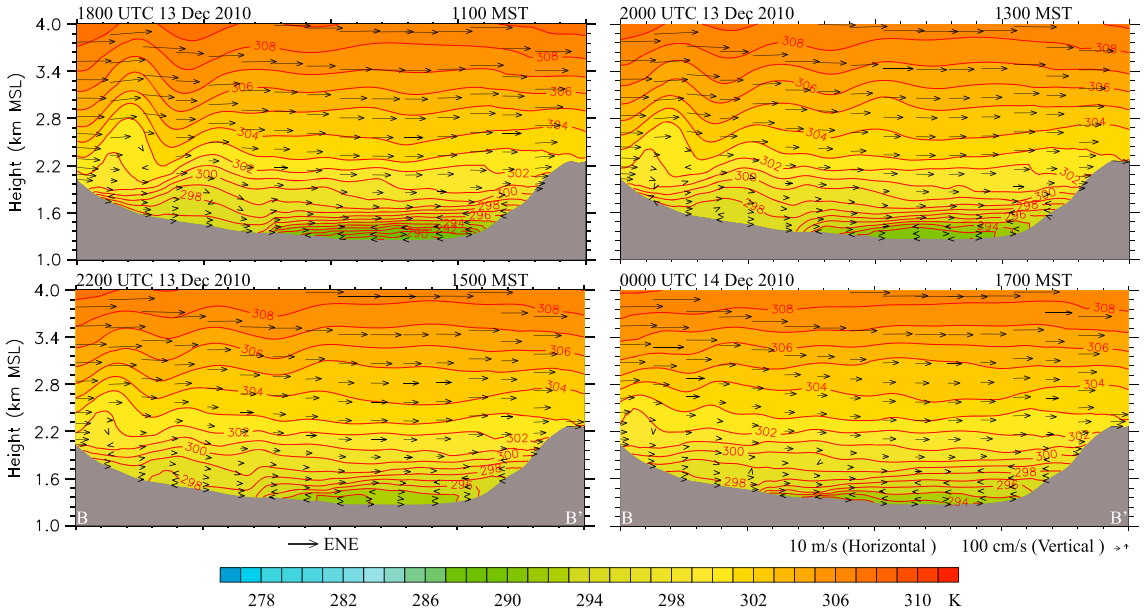

Figure 8. Cross section along BB′ of modeled potential temperature (contours of every 1 K) and wind vectors projected on the cross-sectional plane during the maintenance stage of the cold air pool.

of the valley and into the upper part of the valley, the maintenance stage (0000 UTC 13 December to 1800 UTC 14 December) when the height of the inversion and the temperature and wind in the valley boundary layer do not experience significant change, and the breakup stage (1800 UTC 14 December to 0000 UTC 15 December) when the inversion is lifted and the boundary layer is mixed out. The spatial and temporal variation of the boundary layer structure during the various stages of the CAP episode are revealed by the simulated potential temperatures and wind vectors displayed in cross sections-oriented cross valley (BB′ in Figure 1) and along valley (AA′ in Figure 1).

During the early stage of the CAP buildup, the along-valley cross section (Figure 7a) reveals a valley boundary layer that is moderately stratified. Strong north-northwesterly winds aloft are decoupled from the south-southeasterly flows in the valley by a layer of light wind at the height about the mean elevation of the surrounding mountains (Figure 7a). The winds aloft ahead of a synoptic-scale ridge to the west of the region (see Figures 2b–2d) bring warm air to the region from the northwest, which together with synoptic subsidence, leads to rapid warming as evidenced by the increase of the potential temperature above the valley. Potential temperatures inside the valley also increase with time, and as warm air aloft descends into the valley, the valley atmosphere becomes more stratified. The warming aloft and the increased stratification in the valley boundary layer can also be seen on the cross-valley vertical cross section (Figure 7b). In addition, the cross-valley vertical cross section shows the development of drainage flows in the evening and throughout the night that produces cold air accumulation at the foothills of the Wasatch Range on the east side of the valley.

During the maintenance phase on 13 December (Figure 8), the valley atmosphere is several degrees warmer and the inversion is stronger compared to the previous day. Daytime heating of the valley floor increases the near-surface temperature, producing a shallow mixed layer around 100 m deep in early afternoon (2000 UTC, 1300 MST), becoming slightly deeper later (2200 UTC, 1500 MST).

One interesting feature that occurs during the CAP maintenance phase is the development of a lake breeze on the afternoon of 13 December. The Great Salt Lake serves as a reservoir of cold and damp air and, as shown earlier, the surface inversion develops over the lake surface sooner than in other areas of the valley. The temperature difference between the air above the lake surface and the valley increases significantly during daytime, which together with weak winds and shallow convective boundary layer in the valley, leads to the development of a lake breeze on the afternoon of 13 December. The lake breeze, which begins in the simulation around 1800 UTC and ends at 0200 UTC, travels up valley from northwest to southeast at an average speed of ~2 m s^{-1}. The lake breeze and the associated moisture and temperature transport can be seen in Figure 9, which shows an along-valley vertical cross section (through AA′) of potential temperature, water vapor,

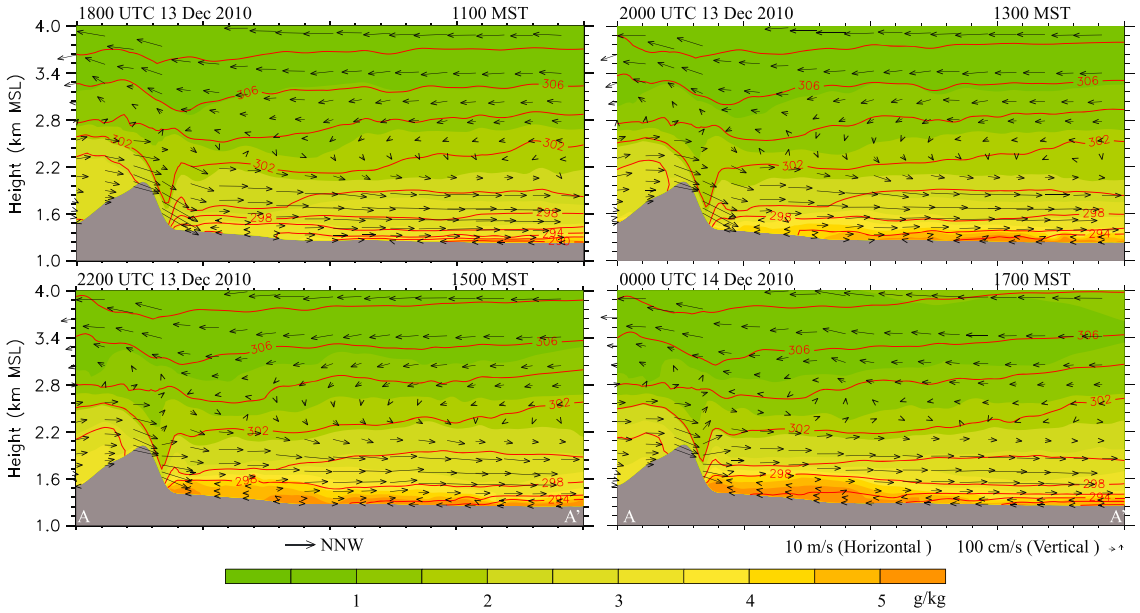

Figure 9. Cross-section along AA′ of modeled potential temperature (contours of every 1 K), mixing ratio (shaded), and wind vectors projected on the cross-sectional plane showing the development of a lake breeze.

and wind vector during the lake breeze event on the afternoon of 13 December. On this day, the valley atmosphere is characterized by stratified conditions with moderate southerly winds in the valley and near-calm conditions above the valley. Near the surface and underneath the layer of southerly flow is a shallow layer of north-northwesterly flow originating from the lake in the northwest and progressing southward in the valley. The lake breeze layer is marked by higher humidity and lower temperature in a shallow mixed layer underneath a stable boundary layer. After the passage of the lake breeze front, the temperature gradient between the northwest and the southeast is weakened significantly. The depth of the lake breeze is 200–300 m.

Zumpfe and Horel [2007] studied a lake breeze along the Great Salt Lake in mid-October. The lake breeze in their study was twice as strong and deep compared to the midwinter lake breeze observed during IOP3. In addition, the lake breeze front, as defined by strong updraft and sharp temperature and moisture gradient, was also more pronounced in the autumn case compared to the winter case. Although both cases had weak synoptic forcing, the autumn case had a much deeper convective boundary layer (1 km) and stronger turbulent mixing [*Cox*, 2006] as well as larger temperature contrast, which may explain the differences in the strength and depth between the autumn and midwinter lake breeze.

The breakup phase of this CAP episode is initiated by the intrusion of a strong southerly flow that is channeled and accelerated through the Jordan Narrow (Figure 10). The southerly flow occupies the lowest 1000 m of the valley with weak synoptic scale winds aloft. With the penetration of this southerly flow, warm air replaces the cold air in the valley, mixing out the inversion. This process begins in the southern end of the valley and progresses northward, gradually at first, but with increasing speed thereafter. Between 1200 and 1600 UTC on 14 December, the leading edge of the warm air moves from the Traverse Range to midvalley. In the next 4 h between 1600 and 2000 UTC, the leading edge of the warm air advances to the northern end of the valley, assisted in part by surface heating. Meanwhile, strong cooling occurs in both the upper part of the valley atmosphere and the overlying atmosphere, which helps to significantly weaken the inversion aloft and eventually lift up the inversion by the end of the period.

4.3. Process Analyses

The results above indicate that the breakup of the CAP can be attributed to the combined effects of synoptic forcing and surface heating. To isolate the relative contribution of solar insolation to the final breakup of this persistent CAP, we present the results of a quasi-idealized experiment in which the shortwave radiation is turned off on the morning of 14 Dec. such that the impact of solar radiation and thus surface heating from sensible heat

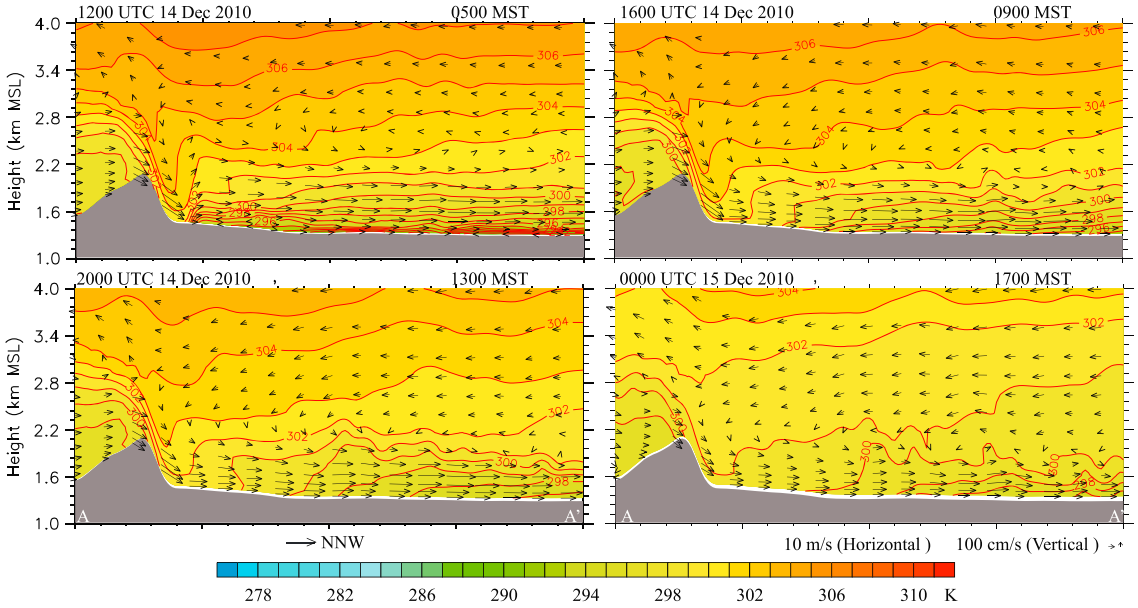

Figure 10. Cross section along AA′ of modeled potential temperature (contours of every 1 K) and wind vectors projected on the cross-sectional plane during the breakup stage of the cold air pool.

flux on CAP breakup is eliminated. The results are shown in Figure 11 for the breakup period. A careful comparison of Figure 11 with Figure 10 reveals several features. The placement of the contours with potential temperature greater than or equal to 300 K is similar in both cases, indicating that the southerly flow and associated warm advection, with cooling above, is sufficient to erode the inversion in the middle and upper valley in the absence of ground heating by solar insolation. However, the lack of surface heating allows for a stronger inversion to develop within the lowest 200 m above the valley floor, especially in the northern part of the valley. It should be noted that sensitivity tests without radiation typically involve simultaneously turning off both solar and terrestrial radiation in order to achieve zero net radiation. When turning off solar radiation only while retaining longwave cooling, as has been done here, the impact of radiation may be overstated.

The above experiment helps to clarify the role of radiation in destroying the wintertime CAP: surface heat flux associated with low-angle radiation is only sufficient for the removal of the near-surface inversion. Wintertime CAPs which are marked by deep inversions are more susceptible to synoptic-scale or regional processes than to local surface processes such as diurnal heating and cooling. This finding agrees with the observational study by *Savoie and McKee* [1995].

To further understand the relative role of synoptic versus surface processes in the evolution of this CAP, process analysis is performed in which the individual factors contributing to the temperature change are estimated and intercompared. According to the thermodynamic energy equation, the change of potential temperature is a

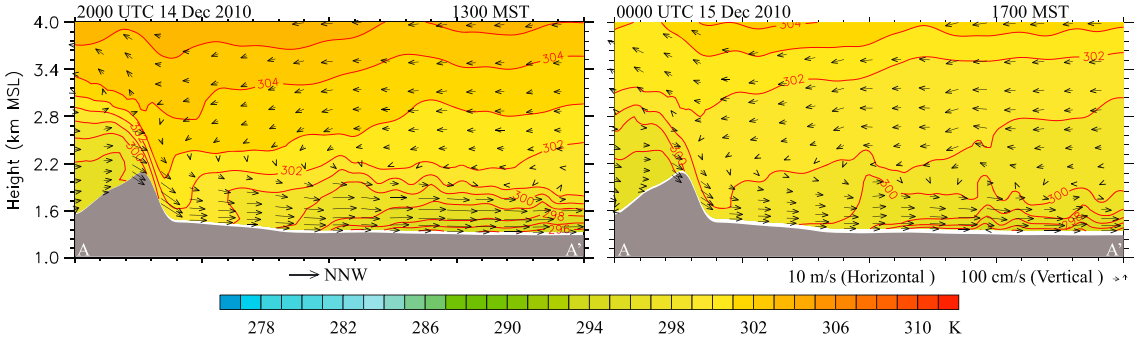

Figure 11. Cross section along AA′ of modeled potential temperature (contours of every 1 K) and wind vectors projected on the cross-sectional plane from the sensitivity experiment with shortwave radiation turned off.

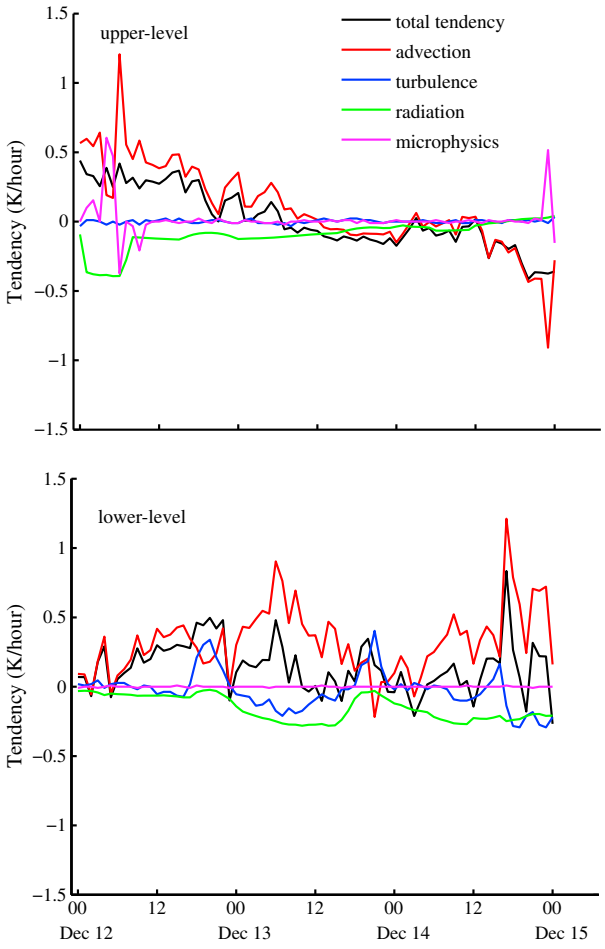

Figure 12. Modeled hourly values of the terms in the thermodynamic equation averaged for the lower (from valley floor to 2000 m msl) and upper layers (3000–4000 msl) at a grid point closest to the ISS site from 0000 UTC 12 December through 0000 UTC 15 December.

result of advection, turbulent diffusion, and diabatic source/sink. The diabatic heating or cooling is associated with clouds and the radiative flux convergence or divergence. Figure 12 shows the various terms in the thermodynamic equation at the grid point closest to the ISS site near the valley center (Figure 1), averaged separately over two layers: lower (from valley floor to 2000 m msl) and upper (~3000–4000 m msl).

The contributions of various terms to the evolution of potential temperature are quite different in the lower and upper layers. In the upper layer, the change of potential temperature is mainly caused by advection, which is relatively large and positive at the beginning, small and variable during the middle period, and relatively large and negative near the end of the episode. The temperature tendency due to radiative flux convergence/divergence is negative throughout the period, while the tendency associated with turbulent diffusion, as expected, is near zero throughout. The variation in the diabatic source/sink associated with cloud microphysics appears to correspond to the presence of lower level clouds at the beginning of the period and high clouds near the end inferred from the model results. There is more variation of the terms in the lower layer throughout the period. The tendency due to radiative flux convergence/divergence is always negative and is larger and more variable compared to the layer aloft. The contribution from the turbulent diffusion term is comparable in magnitude to the advection term and exhibits a diurnal oscillation: small and slightly negative at night and larger and positive in the day. The tendency due to advection is quite variable with values mostly positive.

During the initial phase of CAP buildup (0000 UTC 12 December to 0000 UTC 13 December), the upper layer experiences significant warming which is due entirely to the advection term (including both horizontal advection and subsidence). Warming also occurs in the lower layer due to advection as well as turbulent diffusion. During the maintenance phase (0000 UTC 13 December through 1200 UTC 14 December), temperature in the upper layer is relatively steady with weak cooling due to advection and radiative flux divergence. In contrast, temperature in the lower levels experiences relatively large change in response to the varying advection and turbulence diffusion. It is worth noting that during the daytime on 13 December, evidence of the lake breeze is found in the negative sign of the advection term. Finally, during the breakup phase, there is a small cooling aloft which helps to weaken the stability. What happens in the lower layer during the breakup stage is worthy of additional discussion. During the breakup phase, the advection is very large and positive while turbulent diffusion is large and negative. The warming due to advection associated with the intrusion of the southerly flow overpowers the cooling from downward turbulent flux, leading to a net warming of the lower layer.

The above analyses indicate that the rapid warming of the atmosphere above the valley associated with the synoptic-scale warm advection and subsidence plays a major role in the formation of this persistent CAP, while a combination of cold advection above the valley and the warming of valley air associated with the

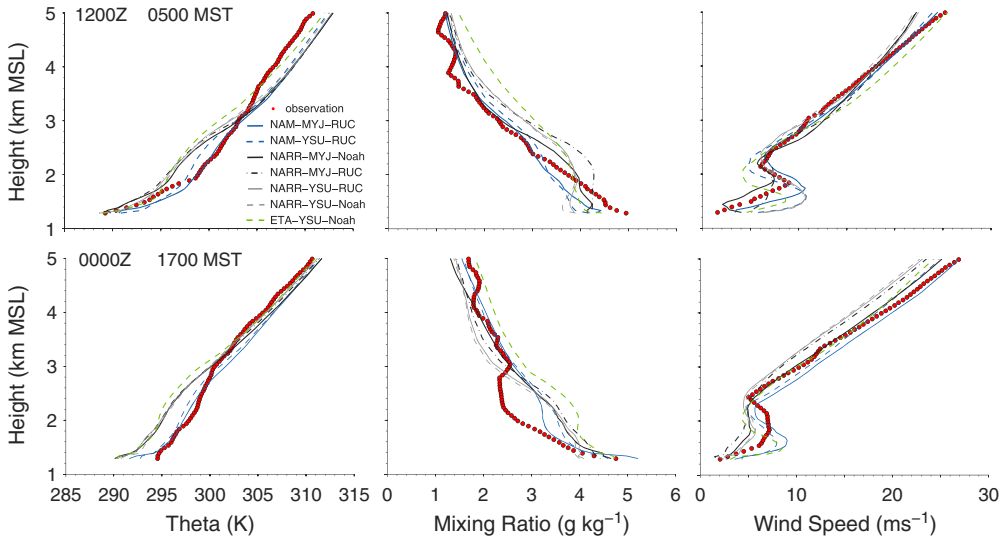

Figure 13. Comparison of the 1200 UTC and 0000 UTC KSLC rawinsonde profiles of potential (left) temperature, (middle) mixing ratio, and (right) wind speed averaged over the simulation period with those from the seven sensitivity simulations.

strong southerly flow intrusion contributes to the removal of the inversion and breakup of the CAP. The surface heating during the day weakens the inversion from below, but its effect alone is insufficient to eliminate the persistent temperature inversion. The lake breeze that develops in the afternoon on 13 December also helps recharge the CAP. This analysis highlights the importance of accurate forecasts of large-scale advection for predicting the buildup and breakup of persistent CAPs in the winter season.

4.4. Sensitivity Study

In this section, results from the seven simulations (Table 1) with different combinations of PBL schemes, LSMs, and large-scale fields are compared with each other and with the observations both at the surface and aloft.

The observational sites are grouped into valley and nonvalley categories according to their locations (see Figure 1). For each category, the bias, correlation coefficients (R), and root-mean-square error (RMSE) between the observed and simulated hourly values are computed to quantify the differences between the simulations and the comparison statistics are shown in Table 1. For temperature, the NAM runs show the smallest bias and smallest RMSE, indicating significantly improved performance when the higher-resolution NAM data set is used to initialize the model and provide boundary conditions, compared to NARR or ETA. Except for NAM-MYJ-RUC, the temperature biases are all negative and range from −3.84 to −0.86°C, which is comparable to what was reported in a case study of a wintertime inversion in interior Alaska, where the near-surface temperatures varied about 4°C depending on the physical parameterization packages used [*Mölders and Kramm*, 2010]. In this study, the difference between valley and nonvalley sites is insignificant. Compared to temperature, R for mixing ratio is lower and only NAM-MYJ-RUC scores over 0.6 while the others score from 0.31 to 0.54. The sign of humidity bias varies among the simulations. The wind speed is overestimated by all simulations, with larger bias associated with the use of the YSU scheme compared to the MYJ scheme in the NARR/ETA group. There is a significant difference between the valley and nonvalley groups for wind speed with considerably higher R for the valley sites than the nonvalley sites. This may be due to the fact that the nonvalley group is comprised of sites of inhomogeneous surfaces and complex terrain, which are not resolved well by the WRF model even at the 500 m grid spacing used in the simulation.

To compare the simulated vertical structure from different combinations, the mean 0000 UTC and 1200 UTC vertical profiles of potential temperature, mixing ratio, and wind speed from each of the seven simulations, averaged over the entire study period, are compared with the time-averaged soundings over the same period from KSLC, with the results shown in Figure 13. All the simulations overestimate the temperature above the valley, and the bias is larger (~2°C) at 1200 UTC than at 0000 UTC. Inside the valley, the NAM runs (blue lines) outperform the NARR (black lines) runs and the ETA (green line) simulation. The NARR and ETA runs significantly underpredict valley temperature with a cold bias as large as 3 K. The NAM runs also appear to

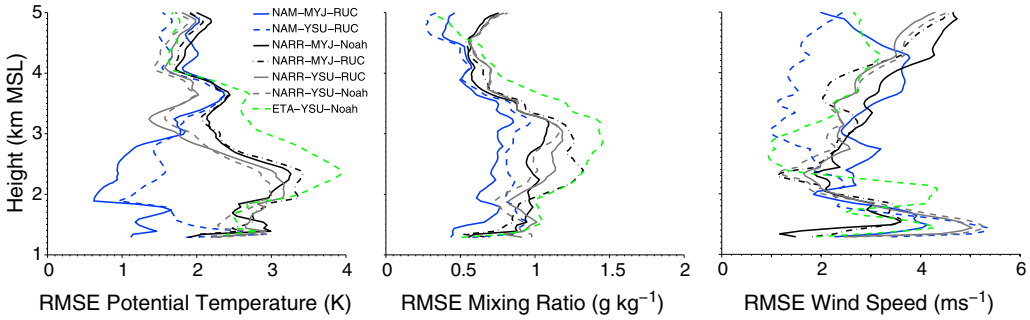

Figure 14. Vertical distribution of the root-mean-square error (RMSE) of the potential (left) temperature, (middle) mixing ratio, and (right) wind speed for the seven sensitivity simulations as compared to the rawinsonde sounding profiles from KSLC.

better simulate the observed vertical structure of moisture and wind speed compared to the NARR/ETA runs. An interesting feature of the rawinsonde wind profiles is a low-level jet (LLJ) with a maximum wind speed at 7–8 m s^{-1} occurring around 1800 m msl (about 400 m agl). There is a diurnal variation of the LLJ characteristics with a sharper jet nose and slightly stronger maximum speed at 1200 UTC compared to 0000 UTC, which is consistent with the diurnal variation of surface stratification and mixing. As shown by the wind profiler observations (Figure 6), LLJ is associated with relatively strong low-level southerly flows driven by regional pressure gradients. Although a drainage flow may also contribute to the formation of a LLJ when it is elevated by a deep inversion [*Renfrew*, 2004; *Vihma et al*., 2011], its contribution to the LLJ here is believed to be small. All the simulations capture the presence of the LLJ, but the simulated jet height and speed vary considerably among the runs with no clear winner. Comparing the MYJ (black dot-dash-dot line) and YSU (gray line) PBL schemes when the same large-scale forcing (NARR) and the same LSM (RUC) are applied, the MYJ scheme tends to produce stronger moisture gradients in the lower boundary layer and thus smaller biases near the surface at 0000 UTC. This may be attributed to weaker vertical mixing strength in the MYJ scheme. These results are consistent with previous studies, where local PBL schemes tend to generate a more realistic stable boundary layer than nonlocal schemes [*Hu et al*., 2010].

The performance skill scores (Figure 14) indicate that NAM-MYJ-RUC yields better results for temperature and mixing ratio while the ETA run scores the lowest. For wind speed, NARR-MYJ-Noah scores the highest in the lower boundary layer and NAM-YSU-RUC performs better in the upper atmosphere.

The influence of the large-scale forcing is further examined by comparing the profiles of potential temperature, specific humidity, and wind speed from the three large-scale model (NAM, ETA, and NARR) analyses utilized in this study to initialize WRF with soundings from KSLC at the time of model initialization (not shown). Although all three model analyses reproduce the observed vertical structure of the atmosphere reasonably well, the NAM analysis appear to give the best agreement while NARR contains slightly larger error. The NARR initial stratification is more stable than what is observed with colder potential temperatures in the lower to middle valley and warmer potential temperatures in the upper valley and above the valley. NARR also significantly overestimates the initial wind speed in the valley and completely fails to describe the observed direction shift from southeast in the lower and middle parts of the valley atmosphere, to northwest in the upper valley and above. All three model analyses exhibit a moist bias especially in midtroposphere from 4000 to 6000 m msl. The lower skill of NARR may be due to its insufficient vertical resolution (28 layers in the archived fields) compared to 40 layers in NAM and 50 layers in ETA. Surface temperature and soil moisture in the three model analyses are similar; however, the difference in soil temperature is very large. The deviation of ETA soil temperature from the observation is as high as 4°C; while it is about 2°C in NARR. The deficiency of ETA and NARR in soil temperature may contribute to the cold bias in both simulated surface and boundary layer temperature discussed earlier. The large differences in the performance scores associated with different large-scale fields imply that the initial/lateral boundary condition data have a significant impact on cold-pool simulation and are thus an important factor to consider when interpreting CAP forecasts.

Although the NAM analyses provide better initial fields and subsequent simulation results compared to the NARR and ETA analyses, the question is whether NAM analysis is adequate to describe the cold pool structure and evolution. Addressing this question is beyond the scope of the current study, but it is unlikely that the

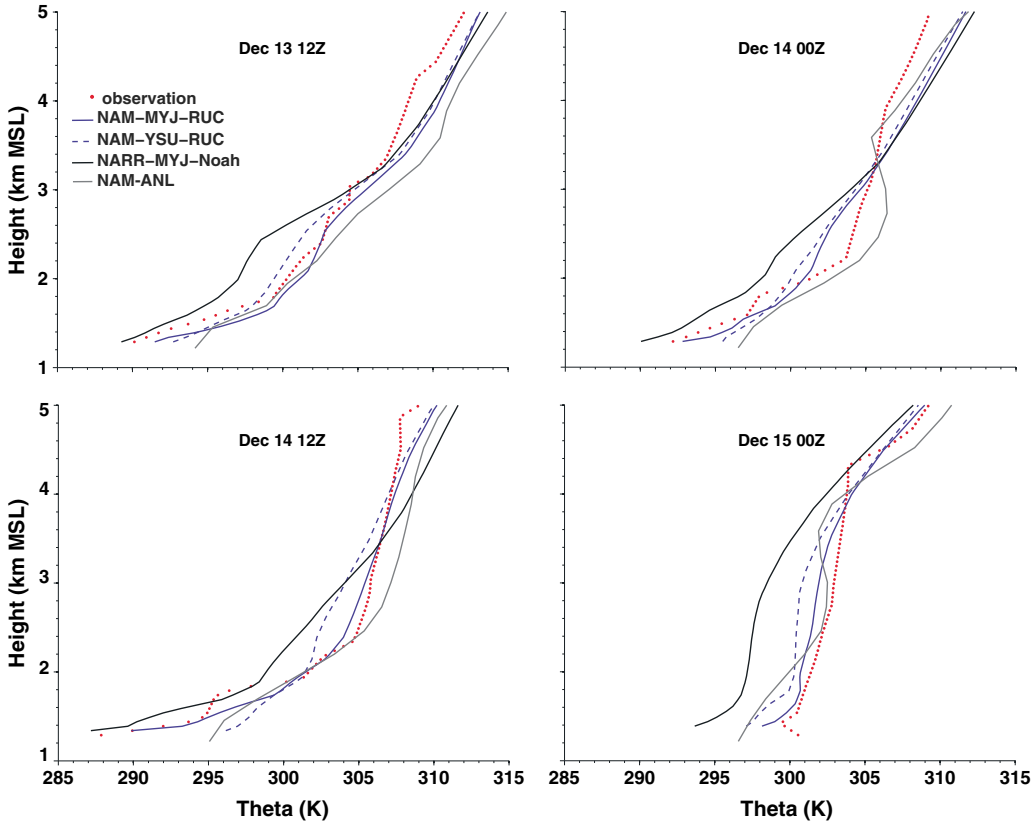

Figure 15. Comparison of profiles of potential temperature interpolated to KSLC from the NAM analyses and from the WRF runs with the KSLC soundings.

12 km resolution of NAM would be sufficient in resolving the details of the terrain and the stable boundary layer structure. An example of this is shown in Figure 15 where vertical profiles of potential temperature interpolated to KSLC from the NAM analyses are compared to the profiles from various WRF runs and with the soundings from KSLC. In all the cases, the NAM analyses show the least skill in reproducing the observed surface inversion and boundary layer structure compared to the WRF runs.

Finally, the ability of the different runs to capture the inversion strength and its evolution during the CAP event is assessed by looking at heat deficit, representing the heat that must be added to destroy an inversion [*Silcox et al.*, 2012; *Whiteman et al.*, 1999]. The normalized heat deficit is calculated as

$$Q = \int_0^h \rho c_p \{[T_h + \Gamma_d(h - z)] - T(z)\} \mathrm{d}z \left[\mathrm{J\ m^{-2}}\right] \quad (1)$$

where ρ is the air density, c_p is the specific heat of air at constant pressure, $\Gamma_d = 0.0098°\mathrm{C\ m^{-1}}$ is the dry adiabatic lapse rate, $h = 1200$ m is the average height of the crest of the confining topography, and $T(z)$ is air temperature. The equation is applied to both the model results and the observations, computed hourly at 60 m vertical resolution for the ISS site (Figure 1) in the center of the valley.

Figure 16 shows a comparison of the observed and the simulated heat deficit. The comparison was grouped by PBL scheme and by large-scale data set to help isolate their contribution to the differences. The results show that between the two PBL schemes, the heat deficit is, on average, little larger with the MYJ scheme compared to that with the YSU scheme, indicating the strength of the simulated inversion by the MYJ scheme is somewhat stronger than that simulated with the YSU scheme. The correlation between the MYJ simulated heat deficit and the observed deficit is higher (0.72) compared to the correlation for the simulation with the YSU scheme (0.5), suggesting that the MYJ scheme is a better choice when it comes to simulating temperature inversion and its evolution. Between the two large-scale data sets, the simulation driven by NAM produces heat deficit that tracks the observed variation of the heat deficit more closely (correlation coefficient 0.82) than the simulation driven

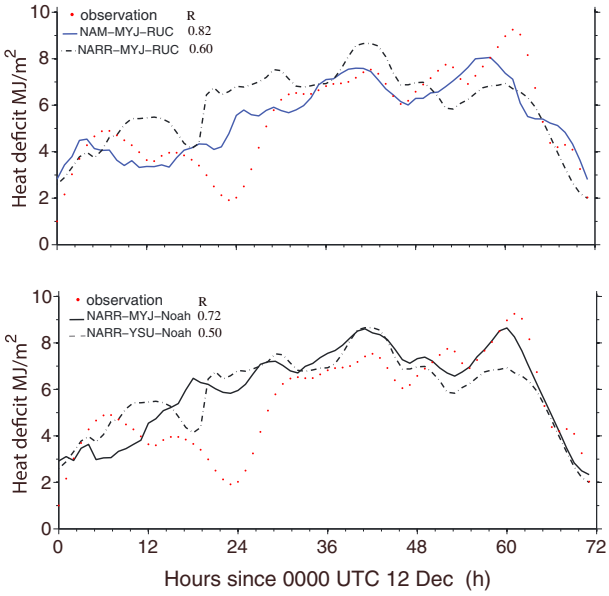

Figure 16. Time series of heat deficit at the ISS site calculated from observations in comparison with the (top) NAM-MYJ-RUC and NARR-MYJ-RUC runs and with the (bottom) NARR-MYJ-Noah and NARR-YSU-Noah runs. *R* is the correlation coefficient between the observation and each simulation.

by NARR (correlation coefficient 0.60). This is consistent with the overall statistical comparison discussed earlier (Table 2). In a recent study that examines the influence of model parameterization schemes and initialization data sets on WRF simulation of a squall line in Kentucky, it was found that a slight preference goes to NAM, although no clearly superior data set is identified [*Gaines*, 2012].

5. Conclusion

In this study, the WRF model (version 3.0) has been used to simulate a persistent CAP episode observed from 12 to 15 December 2010 during the PCAPS (Persistent Cold Air Pool Study) field campaign in Utah's Salt Lake Valley. The model was configured with 500 m horizontal grid spacing, allowing adequate model description of the highly variable terrain in the areas of the Salt Lake Valley. Sensitivity tests were performed to help choose better physical parameterization scheme and large-scale data sets for simulations of CAP events. Observations from a network of surface meteorological stations, rawinsonde soundings, and wind profiler/RASS were used to evaluate the ability of WRF to simulate the CAP characteristics.

The results show that WRF successfully simulated the valley boundary layer structure and evolution during this CAP episode. WRF also captured adequately the timing of the buildup and breakup of the persistent temperature inversion. In addition, WRF reproduced the development of a midwinter lake breeze and its interaction with the CAP. The lake breeze from the Great Salt Lake helps to recharge the CAPs in the Salt Lake Valley. The midwinter lake breeze has lower wind speed and shallower depth compared to a lake breeze observed in autumn.

Process analyses using WRF has provided insight into the physical processes involved in the buildup, maintenance, and breakup of the temperature inversion. Warming of layers above the valley, the result of strong synoptic-scale warm advection and subsidence associated with ridging, was shown to contribute to the formation of the inversion. Regarding the breakdown of the inversion, process analysis showed that low-level warm advection associated with the intrusion of strong southerly flows and simultaneous cooling above the

Table 2. Statistics for Observed and Simulated Surface Temperature, Mixing Ratio, and Wind Speed

		T (°C)			Q (g kg^{-1})			Wind Speed (m s^{-1})		
Experiment Name	Category	*R*	Bias	RMSE	*R*	Bias	RMSE	*R*	Bias	RMSE
NAM-MYJ-RUC	Valley	0.67	0.33	2.29	0.63	−0.04	0.85	0.58	1.46	2.81
	Nonvalley	0.73	0.37	2.28	0.60	0.58	1.30	0.22	0.45	1.86
NAM-YSU-RUC	Valley	0.69	−0.86	2.49	0.31	0.02	0.81	0.56	1.64	2.94
	Nonvalley	0.76	−1.16	2.48	0.46	0.22	0.51	0.16	0.16	1.86
NARR-MYJ-Noah	Valley	0.68	−2.65	3.40	0.42	0.15	0.84	0.38	0.32	1.79
	Nonvalley	0.61	−1.74	3.07	0.39	−0.17	0.62	0.23	1.18	2.23
NARR-MYJ-RUC	Valley	0.73	−3.56	4.09	0.51	0.11	0.50	0.46	0.20	1.83
	Nonvalley	0.53	−3.76	4.83	0.44	−0.07	0.50	0.28	0.60	1.82
NARR-YSU-RUC	Valley	0.69	−3.18	3.88	0.40	−0.07	0.52	0.50	1.01	2.53
	Nonvalley	0.58	−3.84	4.96	0.39	−0.27	0.59	0.14	0.06	1.62
NARR-YSU-Noah	Valley	0.63	−1.91	3.13	0.54	−0.54	0.81	0.49	1.15	2.68
	Nonvalley	0.64	−2.68	3.77	0.34	−0.25	0.74	0.16	0.36	1.97
ETA-YSU-Noah	Valley	0.68	−3.05	3.76	0.54	−0.14	0.60	0.53	0.78	2.13
	Nonvalley	0.52	−2.37	3.83	0.48	0.00	0.61	0.22	0.64	1.84

valley associated with synoptic cold advection helped mix out the inversion in the valley and lift the subsidence inversion near the top of the valley. Numerical experiments with/without solar insolation during the inversion breakup indicate that the heating on the ground generated by the low-angle solar radiation in midwinter is only sufficient for the removal of the near-surface inversion.

Comparisons of results from WRF simulations with various combinations of boundary layer schemes, land surface models, and large-scale forcing fields yielded similar results with regard to overall development of the CAP episode, suggesting that the CAP characteristics are not very sensitive to the choices of these model parameters. However, detailed analyses revealed considerable differences in the statistical measures of the model performance (biases, RMSE, and correlations), and the results suggest that better results are achieved when WRF is driven by high-resolution NAM fields compared to NARR or ETA fields and that the combination of NAM fields, MYJ PBL scheme, and the RUC surface model appears to perform better overall.

Although previous numerical studies, such as *Zhong et al*. [2001], *Billings et al*. [2006], and most recently *Wei et al*. [2013] also simulated persistent CAP episodes, these studies are limited by relatively coarse model resolution and the availability of only routine observations for model validation. The availability of data from an intensive field campaign designed specifically for CAP study allowed for more detailed analyses and model comparison, especially in the boundary layer above the surface. The results from this study add to our knowledge about CAP structure and evolution, the processes involved in its formation and destruction, the ability of community mesoscale models in simulating these processes, and the influence of physical parameterization schemes and large-scale data sets on the mesoscale model simulations. Future work will involve simulating more CAP cases under different conditions such as cloud cover and snow on the ground and identify other physical processes that may be important for CAP.

Acknowledgments

This research was supported by the U.S. National Science Foundation under grant ATM0938401. Any opinions, findings, and conclusions or recommendations expressed in this materials are those of authors and do not necessarily reflect the views of the National Science Foundation. We wish to thank all PCAPS participants for making the PCAPS data available, and E. Crosman, N. Lareau, C.D. Whiteman, J. Horel, and S. Hoch for many useful discussions. We also wish to thank M.T. Kiefer for his assistance in editing the paper as well as the three anonymous reviewers for their constructive comments. The computational resources were provided by the computational and information systems laboratory at the National Center for Atmospheric Research, sponsored by the National Science Foundation and other agencies.

References

Allwine, K. J., B. K. Lamb, and R. Eskridge (1992), Wintertime dispersion in a mountainous basin at Roanoke, Virginia: Tracer study, *J. Appl. Meteorol.*, *31*, 1295–1311.

Anquetin, S., C. Guilbaud, and J.-P. Chollet (1998), The formation and destruction of inversion layers within a deep valley, *J. Appl. Meteorol.*, *37*, 1547–1560.

Bader, D. C., and T. B. McKee (1983), Dynamical model simulation of the morning boundary layer development in deep mountain valleys, *J. Appl. Meteorol. Climatol.*, *22*(3), 341–351.

Bader, D. C., and T. B. McKee (1985), Effect of shear, stability and valley characteristics on the destruction of temperature inversions, *J. Clim. Appl. Meteorol.*, *24*, 822–832.

Banta, R. M. (1984), Daytime boundary-layer evolution over mountainous terrain. Part I: Observations of the dry circulations, *Mon. Weather Rev.*, *112*, 340–356.

Billings, B. J., V. Grubišić, and R. D. Borys (2006), Maintenance of a mountain valley CAP: A numerical study, *Mon. Weather Rev.*, *134*(8), 2266–2278.

Chen, F., and J. Dudhia (2001), Coupling an advanced land surface hydrology model with the Penn State-NCAR MM5 modeling system. Part I: Model implementation and sensitivity, *Mon. Weather Rev.*, *129*, 569–585.

Clements, C. B., C. D. Whiteman, and J. D. Horel (2003), Cold-air-pool structure and evolution in a mountain basin: Peter Sinks, Utah, *J. Appl. Meteorol.*, *42*(6), 752–768.

Cox, J. A. W. (2006), *The Sensitivity of Thermally Driven Mountain Flows to Land Cover Change*, 90 pp., The Univ. of Utah, Salt Lake City.

Eisenbach, S., B. Pospichal, C. D. Whiteman, R. Steinacker, and M. Dorninger (2003), Classification of CAP events in the Gstettneralm, a sinkhole in the Eastern Alps, paper presented at Int. Conf. on Alpine Meteorology and MAP-Meeting, MeteoSwiss, Publication, Brig, Switzerland.

Gaines, M. (2012), *Application of the Weather Research and Forecasting (WRF) Model to Simulate a Squall Line: Implications of Choosing Parameterization Scheme Combinations and Model Initialization Data Sets*, Western Kentucky Univ., Bowling Green.

Hill, C. D. (1993), Forecast problems in the western region of the National Weather Service: An overview, *Weather Forecast.*, *8*, 158–165.

Hong, S.-Y., Y. Noh, and J. Dudhia (2006), A new vertical diffusion package with explicit treatment of entrainment processes, *Mon. Weather Rev.*, *134*, 2318–2341.

Horel, J., M. Splitt, L. Dunn, J. Pechmann, B. White, C. Ciliberti, S. Lazarus, J. Slemmer, D. Zaff, and J. Burks (2002), Mesowest: Cooperative mesonets in the western United States, *Bull. Am. Meteorol. Soc.*, *83*, 211–225.

Hu, X., J. W. Nielsen-Gammon, and F. Zhang (2010), Evaluation of three planetary boundary layer schemes in the WRF model, *J. Appl. Meteorol. Climatol.*, *49*, 1831–1844.

Janjic, Z. I. (1990), The step-mountain coordinate: Physical package, *Mon. Weather Rev.*, *118*, 1429–1443.

Janjic, Z. I. (1994), The step-mountain Eta coordinate model: Further developments of the convection, viscous layer, and turbulence closure schemes, *Mon. Weather Rev.*, *122*, 927–945.

Janjic, Z. I. (2001), Nonsingular implementation of the Mellor-Yamada level 2.5 scheme in the NCEP meso model, NOAA/NWS/NCEP Office Note 437, 61 pp.

Kondo, J., T. Kuwagata, and S. Haginoya (1989), Heat budget analysis of nocturnal cooling and daytime heating in a basin, *J. Atmos. Sci.*, *46*(19), 2917–2933.

Kossmann, M., A. P. Sturman, P. Zawar-Reza, H. A. McGowan, A. J. Oliphant, I. F. Owens, and R. A. Spronken-Smith (2002), Analysis of the wind field and heat budget in an alpine lake basin during summertime fair weather conditions, *Meteorol. Atmos. Phys.*, *81*(1-2), 27–52.

Kudoh, T., H. Tanaka, H. Toritani, and S. Hwang (1982), Formation of cold air lake in Sugadaira Basin, *Geogr. Rev. Jpn.*, *55*, 849–856.

Lareau, N. P., E. Crosman, C. D. Whiteman, J. D. Horel, S. W. Hoch, W. O. J. Brown, and T. W. Horst (2013), The persistent CAP study, *Bull. Am. Meteorol. Soc.*, *94*, 51–63.

Magono, C., C. Nakamura, and Y. Yoshida (1982), Nocturnal cooling of the Moshiri Basin, Hokkaido in midwinter, *J. Meteorol. Soc. Jpn.*, *60*, 1106–1116.
Mellor, G. L., and T. Yamada (1982), Development of a turbulence closure model for geophysical fluid problems, *Rev. Geophys.*, *20*, 851–875.
Mölders, N., and G. Kramm (2010), A case study on wintertime inversions in Interior Alaska with WRF, *Atmos. Res.*, *95*(2–3), 314–332.
Nakamura, C., and C. Magono (1982), The extremely low temperature in Hokkaido, Japan, during 1976–77 winter, and its numerical simulation, *J. Meteorol. Soc. Jpn.*, *60*, 956–966.
Pataki, D. E., B. J. Tyler, R. E. Peterson, A. P. Nair, W. J. Steenburgh, and E. R. Pardyjak (2005), Can carbon dioxide be used as a tracer of urban atmospheric transport?, *J. Geophys. Res.*, *110*, D15102, doi:10.1029/2004JD005723.
Petkovsek, Z. (1978), Relief meteorologically relevant characteristics of basins, *Z. Meteorol.*, *28*, 333–340.
Petkovsek, Z. (1980), Additional relief meteorologically relevant characteristics of basins, *Z. Meteorol.*, *30*, 379–382.
Petkovsek, Z. (1992), Turbulent dissipation of cold air lake in a basin, *Meteorol. Atmos. Phys.*, *47*, 237–245.
Rakovec, J., J. Merše, S. Jernej, and B. Paradiž (2002), Turbulent dissipation of the CAP in a basin: Comparison of observed and simulated development, *Meteorol. Atmos. Phys.*, *79*(3–4), 195–213.
Reeves, H. D., and D. J. Stensrud (2009), Synoptic-scale flow and valley CAP evolution in the western United States, *Weather Forecast.*, *24*(6), 1625–1643.
Reeves, H. D., K. L. Elmore, G. S. Manikin, and D. J. Stensrud (2011), Assessment of forecasts during persistent valley CAPs in the Bonneville Basin by the North American Mesoscale model, *Weather Forecast.*, *26*, 447–467.
Renfrew, I. A. (2004), The dynamics of idealized katabatic flow over a moderate slope and ice shelf, *Q. J. R. Meteorol. Soc.*, *130*, 1023–1045.
Sakiyama, S. K. (1990), Drainage flow characteristics and inversion breakup in two Alberta mountain valleys, *J. Appl. Meteorol.*, *29*, 1015–1030.
Savoie, M. H., and T. B. McKee (1995), The role of wintertime radiation in maintaining and destroying stable layers, *Theor. Appl. Climatol.*, *52*, 43–54.
Silcox, G. D., K. E. Kelly, E. T. Crosman, C. D. Whiteman, and B. L. Allen (2012), Wintertime PM2.5 concentrations during persistent, multi-day CAPs in a mountain valley, *Atmos. Environ.*, *46*, 17–24.
Skamarock, W. C., J. B. Klemp, J. Dudhia, D. O. Gill, D. M. Barker, W. Wang, and J. G. Powers (2005), A description of the advanced research WRF version 2, *NCAR Tech Notes-468+STR*.
Smirnova, T. G., J. M. Brown, S. G. Benjamin, and D. Kim (2000), Parameterization of cold-season processes in the MAPS land-surface scheme, *J. Geophys. Res.*, *105*, 4077–4086.
Smith, R., et al. (1997), Local and remote effects of mountains on weather: Research needs and opportunities, *Bull. Am. Meteorol. Soc.*, *78*, 877–892.
Smith, S. A., A. R. Brown, S. B. Vosper, P. A. Murkin, and A. T. Veal (2010), Observations and simulations of CAPing in valleys, *Boundary Layer Meteorol.*, *134*, 85–108.
Steinacker, R., C. D. Whiteman, M. Dorninger, B. Pospichal, S. Eisenbach, A. M. Holzer, P. Weihs, E. Mursch-Radlgruber, and K. Baumann (2007), A sinkhole field experiment in the Eastern Alps, *Bull. Am. Meteorol. Soc.*, *88*, 701–716.
Struthwolf, M. (2005), An evaluation of fog forecasting tools for a fog event and non-event at Salt Lake City International Airport, *Rep*.
Sturman, A. P., et al. (2003a), Supplement to the Lake Tekapo Experiment (LTEX): An investigation of atmospheric boundary layer processes in complex terrain, *Bull. Am. Meteorol. Soc.*, *84*, 381–383.
Sturman, A. P., et al. (2003b), The Lake Tekapo Experiment (LTEX): An investigation of atmospheric boundary layer processes in complex terrain, *Bull. Am. Meteorol. Soc.*, *84*(3), 371–380.
Vihma, T., T. Kilpeläinen, M. Manninen, A. Sjöblom, E. Jakobson, T. Palo, J. Jaagus, and M. Maturilli (2011), Characteristics of temperature and humidity inversions and low-level jets over Svalbard Fjords in spring, *Adv. Meteorol.*, *2011*, Article 486807, doi:10.1155/2011/486807.
Vrhovec, T. (1991), A cold air lake formation in a basin-a simulation with a mesoscale numerical model, *Meteorol. Atmos. Phys.*, *46*, 91–99.
Vrhovec, T., and A. Hrabar (1996), Numerical simulations of dissipation of dry temperature inversions in basins, *Geofizika*, *13*, 81–96.
Wei, L., Z. Pu, and S. Wang (2013), Numerical simulation of the life cycle of a persistent wintertime inversion over Salt Lake City, *Boundary Layer Meteorol.*, *148*, 399–418.
Whiteman, C. D., X. Bian, and S. Zhong (1999), Wintertime evolution of the temperature inversion in the Colorado Plateau Basin, *J. Appl. Meteorol.*, *38*, 1103–1117.
Whiteman, C. D., S. Zhong, W. J. Shaw, J. M. Hubbe, X. Bian, and J. Mittelstadt (2001), CAPs in the Columbia basin, *Weather Forecast.*, *16*(4), 432–447.
Whiteman, C. D., S. Eisenbach, B. Pospichal, and R. Steinacker (2004a), Comparison of vertical soundings and sidewall air temperature measurements in a small Alpine basin, *J. Appl. Meteorol.*, *43*, 1635–1647.
Whiteman, C. D., T. Haiden, B. Pospichal, S. Eisenbach, and R. Steinacker (2004b), Minimum temperatures, diurnal temperature ranges, and temperature inversions in limestone sinkholes of different sizes and shapes, *J. Appl. Meteorol.*, *43*(8), 1224–1236.
Whiteman, C. D., B. Pospichal, S. Eisenbach, P. Weihs, C. B. Clements, R. Steinacker, E. Mursch-Radlgruber, and M. Dorninger (2004c), Inversion breakup in small Rocky Mountain and alpine basins, *J. Appl. Meteorol.*, *43*(8), 1069–1082.
Whiteman, C. D., et al. (2008), METCRAX 2006: Meteorological experiments in Arizona's Meteor Crater, *Bull. Am. Meteorol. Soc.*, *89*, 1665–1680.
Wolyn, P. G., and T. B. Mckee (1989), Deep stable layers in the intermountain western United State, *Mon. Weather Rev.*, *117*, 461–472.
Yao, W., and S. Zhong (2009), Nocturnal temperature inversions in a small, enclosed basin and their relationship to ambient atmospheric conditions, *Meteorol. Atmos. Phys.*, *103*, 195–210.
Zängl, G. (2003), The impact of upstream blocking, drainage flow and the geostrophic pressure gradient on the persistence of CAPs, *Q. J. R. Meteorol. Soc.*, *129*(587), 117–137.
Zängl, G. (2005a), Wintertime CAPs in the Bavarian Danube Valley Basin: Data analysis and idealized numerical simulations, *J. Appl. Meteorol.*, *44*(12), 1950–1971.
Zängl, G. (2005b), Dynamical aspects of wintertime CAPs in an Alpine valley system, *Mon. Weather Rev.*, *133*(9), 2721–2740.
Zängl, G. (2005c), Formation of extreme CAPs in elevated sinkholes: An idealized numerical process study, *Mon. Weather Rev.*, *133*(4), 925–941.
Zhong, S., C. D. Whiteman, X. Bian, W. J. Shaw, and J. M. Hubbe (2001), Meteorological processes affecting the evolution of a wintertime CAP in the Columbia Basin, *Mon. Weather Rev.*, *129*(10), 2600–2613.
Zumpfe, D. E., and J. D. Horel (2007), Lake-breeze fronts in the Salt Lake Valley, *J. Appl. Meteorol. Climatol.*, *46*, 196–211.